ARTICLE

Effect of gamma radiolysis on pit initiation of zircaloy-2 in water containing sea salt

Takafumi Motooka[a*], Atsushi Komatsu[a], Takashi Tsukada[a] and Masahiro Yamamoto[a]

[a] *Japan Atomic Energy Agency, 2-4 Shirane, Shirakata, Tokai-mura, Naka-gun, Ibaraki 319-1195, Japan*

(Received)

In spent fuel pools at the Fukushima Daiichi Nuclear Power Station (1F), seawater was injected for cooling purposes after the tsunami disaster in March of 2011. It is well known that the chloride in the seawater has the potential to cause localized corrosion (e.g., pitting corrosion) in metals. In this study, we evaluated the pitting potentials of zircaloy-2, the material used in the fuel cladding tubes in 1F, as a function of chloride concentration. To accomplish this, we used artificial seawater under gamma-ray irradiation and investigated the effect of radiolysis on pit initiation of zircaloy-2 in water containing sea salt. Changes in the composition of water containing sea salt were analyzed as well, both before and after gamma-ray irradiation. The characteristics of the resultant oxide films formed on zircaloy-2 were evaluated by X-ray photoelectron spectroscopy and electrochemical impedance spectroscopy. The experimental results showed that the pitting potential under irradiation was slightly higher than that under conditions in which no radiation was present, and that the pitting potential decreased with increasing chloride concentration in the presence as well as the absence of radiation. Solution

[*]Corresponding author, E-mail: motoka.takafumi@jaea.go.jp

analyses for water containing sea salt showed that hydrogen peroxide was generated by irradiation. The oxide film was composed of zirconium oxide and was made thicker during the irradiation. The higher pitting potential could thus be explained by the capacity of hydrogen peroxide to oxidize the surface and enhance oxide film formation. Under gamma-ray irradiation, the zircaloy-2 surface with an oxide film formed by radiolysis products was found to be resistant to pitting in the presence of chloride.

Keywords; pitting corrosion; zircaloy-2; sea salt; artificial seawater; gamma rays; irradiation; chloride; hydrogen peroxide; radiolysis

1. Introduction

On March 11, 2011, the Fukushima Daiichi Nuclear Power Station (1F) lost electrical power due to the Great East Japan Earthquake. As a result, the cooling functions normally used for spent fuel pools (SFPs) were no longer sufficient under the circumstances. As an emergency measure, seawater was injected into the SFPs of units 2, 3, and 4 in order to cool the spent fuel. Ultimately, this led to a high chloride concentration in the water in SFPs. In the early stages of repair following the tsunami, the maximum chloride concentration in the water of the SFPs was estimated to be approximately 2500 ppm [1]. When the levels were measured in August 2011, the chloride concentrations of units 2, 3, and 4 were 1508, 1769, and 1944 ppm, respectively [2]. In October 2012, the chloride concentration had decreased to less than 20 ppm as a result of desalination [3]. Here, we note that spent and unused fuels have been stored in the SFPs at 1F.

The nuclear reactor at 1F is a boiling water reactor. Zircaloy-2 (Zry-2) was adopted as cladding material for the tubes owing to its low thermal neutron capture cross-section, good mechanical properties, and adequate corrosion resistance in high temperature water [4]. It is well known that the corrosion resistances of zirconium and zirconium alloy originate from the formation of a protective passive film composed of zirconium oxides. However, zirconium and zirconium alloy are still susceptible to pitting corrosion in chloride solutions with powerful oxidants [5]-[7]. Spent fuels stored in the SFP were hot and highly radioactive, and thus, radiated alpha, beta, and gamma rays. The radiation field such as that present in the SFP was capable of causing water to decompose into highly oxidizing species (e.g., H_2O_2 and OH•) [8]. In the case of water containing sea salt, chloride induced species (e.g., ClO_2^- and ClO_3^-) would be generated as radiolysis products [9]. These oxidizing species are capable of promoting corrosion in stainless steel [10] and, furthermore, it is believed that these particular radiolysis products might affect the pitting corrosion behavior of Zry-2. However, the effect of the radiolysis products of water containing sea salt on the pitting corrosion of Zry-2 is not well known.

In this study, we have conducted electrochemical measurements using artificial seawater and gamma rays (Co-60 source) in order to evaluate the effect of radiolysis on pit initiation in zircaloy-2 in water containing sea salt. Pitting potentials of Zry-2 were measured as a function of chloride concentration in the presence as well as the absence of gamma rays. The changes in composition of water containing sea salt were analyzed before and after the irradiation in order to determine quantities of stable radiolysis products. In order to better identify the effects of radiolysis on a Zry-2 surface, the characteristics of an oxide film formed on bare Zry-2 both with and without gamma-ray radiation was examined using electrochemical impedance spectroscopy (EIS) on pre-irradiated Zry-2 in artificial seawater. The chemical states of elements and the thickness of the oxide films formed on the Zry-2 were evaluated through X-ray photoelectron spectroscopy (XPS).

2. Experimental

2.1. Test solutions

Test solutions were artificial seawater (ASW) and ASW diluted with distilled water. ASW was prepared using a reagent: Aquamarin (Yashima Pure Chemical Co. Ltd.). **Table 1** shows the chemical composition of the ASW. The chloride concentration was 19000 ppm.

<Table 1>

2.2. Material and specimen

Specimens were composed of an 11-mm-diameter Zry-2 rod in as-received condition. **Table 2** lists the chemical composition of the Zry-2 rod. For electrochemical measurements, the specimen was connected to a 3-mm-diameter zirconium rod covered with an insulating tube. The dimensions of the specimen are shown in **Figure 1**.

<Table 2>

<Figure 1>

2.3. Solution analyses

The concentrations of hydrogen peroxide (H_2O_2) in test solutions were analyzed via the enzyme method using tetra-aminoantipyrine with an absorption spectrophotometer (Rambda-9000™; Kyoritsu Chemical-check Lab., Corp.). The concentrations of HClO and ClO^- in test solutions were analyzed using the DPD method. The concentrations of other anions in the test solutions were measured via ion chromatography with an ion chromatograph system (IC-883™; Metrohm Inc.). The lower limit of detection for anions (e.g., ClO_2^-, ClO_3^-, and BrO_3^-) was approximately 0.02 ppm.

2.4. Electrochemical measurements

A potentiostat (Reference 600™; GAMRY Inst.) was used for electrochemical measurements. The electrochemical test cell comprised a three-electrode system. The working electrode was either a platinum plate or a Zry-2 specimen, the counter electrode was a platinum plate, and the reference electrode was a saturated KCl Ag/AgCl electrode (abbreviated as SSE). Prior to electrochemical measurements, a test solution was aerated. In this paper, potential values were expressed with respect to SSE (+0.199 V vs. SHE at 298 K).

In our previous study, H_2O_2 at a level of a few ppm was detected in the ASW after gamma-ray irradiation for 1 h [11]. In order to evaluate the oxidation power of H_2O_2, cathodic polarization curves of platinum in the ASW with and without H_2O_2 at room temperature were measured and analyzed.

Anodic polarization curves of Zry-2 in test solutions (where a pit was forcibly generated by applying voltage) were obtained to determine the pitting potential (pit initiation potential). First, the open circuit potential (OCP) was measured, followed by a potentiodynamic polarization curve which was recorded at a scan rate of 0.333 mV/s. The pitting potential (E_{pit}) was determined as the potential at which a rapid increase in current was observed. Over E_{pit}, passive film can be broken down and metals cause pitting corrosion. Zry-2 specimens were polished with an abrasive 600 grade SiC paper. After degreasing the specimens with acetone,

we conducted measurements immediately on some while others were immersed in test solutions and measured after given periods of time.

Electrochemical impedance spectroscopy (EIS) was employed to obtain polarization resistances, double layer capacitance, and film thicknesses. EIS was conducted at a sinusoidal voltage perturbation of 10 mV over a frequency range of 10^{-2}–10^{5} Hz. Polarization resistance, double layer capacitance, and film thickness were determined by using Echem Analyst™ Software (GAMRY Inst. Inc.). Some specimens were pre-irradiated in ASW while others were just immersed in ASW prior to EIS measurements.

2.5. Gamma-ray irradiation

Gamma-ray irradiation was conducted in the Co-60 irradiation facility at Takasaki Advanced Radiation Research Institute of the Japan Atomic Energy Agency.

In the case of electrochemical measurements, an electrochemical test cell was set inside a concrete cell with a Co-60 source. The electrochemical test cell inside the concrete cell was connected to the potentiostat outside the concrete cell by 10-m-long cables. The dose rate for a specimen was controlled at levels of approximately 500 or 5000 Gy/h by varying the distance from the Co-60 source. The dose rate was within the range of dose rates in the SFPs at 1F [12]. The dose rate at the location of the test specimen was determined using an alanine dosimeter (Aminogray; Hitachi Cable, Ltd.). The temperature of the test solutions was not controlled and ranged from 298 to 303 K irrespective of the irradiation. For solution analyses, test solutions in closed glass tubes were irradiated. In the preparation of samples for EIS and X-ray photoelectron spectroscopy, some specimens were pre-irradiated in a test solution for a given amount of time.

2.6. XPS analysis of oxide film on zircloy-2

To investigate the characteristics of the oxide film formed on the Zry-2 surface, the

oxide films formed in the ASW in both the presence and absence of radiation were analyzed via X-ray photoelectron spectroscopy (XPS) using a PHI Quantera SXM ^{TM} (ULVAC-PHI, Inc.). Al Kα radiation with an acceleration voltage of 1486.6 eV was used at a pass energy of 23.5 eV. The incident beam diameter was 200 μm. We monitored Zr 3d and O 1s. Depth profiling was conducted using an ion gun (Ar^+, 2 keV).

3. Results and Discussion

3.1. Solution analyses

A closed glass tube filled with ASW containing 6.5 ppm of dissolved oxygen was irradiated at dose rates of 500 and 5000 Gy/h at room temperature for up to 100 h. **Figure 2** shows the relationship between H_2O_2 concentration and irradiation time. H_2O_2 was detected at a level of approximately 3 ppm after irradiation for 3 h. For higher dose rates, a steady composition of H_2O_2 was reached more quickly and resulted in a higher final overall concentration. The concentration of HClO and ClO^- in test solutions was under the detection limit (<0.05 ppm). **Figure 3** shows the chromatogram of ASW after irradiation for 100 h at a dose rate of 5000 Gy/h. The obvious peaks were Cl^- and SO_4^{2-}. The concentrations of chloride and bromide induced species (e.g., ClO_2^-, ClO_3^- and BrO_3^-) were below the lower limit of detection. The chromatogram of ASW after irradiation for 100 h at a dose rate of 500 Gy/h had a similar profile. No additional anions besides those already present in ASW were detected following the irradiation. Kelm conducted an irradiation test for a concentrated NaCl solution, which has a higher chloride concentration than ASW. He reported that for NaCl at a concentration of less than 2 mol/L, yields of ClO_3^-, ClO_2^-, and ClO^- were close to zero: near the micro-mole per liter range detection limit [15]. These results demonstrated that H_2O_2 was the dominant long-lived stable radiolysis product in ASW under irradiation conditions.

<Figure 2>

<Figure 3>

3.2. Cathodic polarization curves for platinum in artificial seawater

Figure 4 shows cathodic polarization curves of platinum in ASW in the absence and presence of H_2O_2 at a concentration of 30 ppm and a temperature of 298 K. ASWs had 6.5 ppm of dissolved oxygen (DO). The OCP in the presence of H_2O_2 at 30 ppm was approximately 0.04 V higher than that in the absence of H_2O_2. The diffusion limiting current density in the presence of H_2O_2 was approximately 60 $\mu A/cm^2$, and was about 3 times greater than that in the absence of H_2O_2. The presence of H_2O_2 in ASW caused the solution to become oxidizing. The main cathodic reactions in the presence and absence of H_2O_2 were as follows [13], [14]:

In the presence of H_2O_2 $\quad H_2O_2 + 2e^- \rightarrow 2OH^-$ (1)

In the absence of H_2O_2 $\quad 2H_2O + O_2 + 4e^- \rightarrow 4OH^-$ (2)

In tested solutions, the molar ratio of H_2O_2 to O_2 was (30/34) to (6.5/32): 4.3 to 1. According to equations (1) and (2), it was expected that the cathodic current (diffusion limiting current) measured in ASW with H_2O_2 at 30 ppm and DO at 6.5 ppm was approximately 3.2 times greater than that in ASW without H_2O_2. This is in good agreement with the experimental result.

<Figure 4>

3.3. Chronopotentiometry of zircaloy-2

Figure 5 shows typical chronopotentiometry plots obtained from the initial dipping of the specimens into room temperature ASW over a period of 100 h. Two were plots for Zry-2 in the absence of radiation and the others were for Zry-2 in the presence of radiation at dose rates of 500 and 5000 Gy/h. Solid lines indicate radiation and dotted lines indicate the case in which no radiation was present. In all cases, the OCP was initially the more active (cathodic) side, but it stabilized to nobler value as immersion time increased. The OCP without radiation in the absence of H_2O_2 at 100 h was -0.22 V, and the OCPs in the presence of radiation at dose rates of 500 and 5000 Gy/h were -0.16 and -0.11 V, respectively. The OCP in ASW containing H_2O_2 at 30 ppm without irradiation was -0.13 V. The test solution irradiated over a period of 100 h at 500 Gy/h contained H_2O_2 at 1.8 ppm, and that solution irradiated over a period of 100 h at

5000 Gy/h contained H_2O_2 at 2.9 ppm. These results suggest that the presence of oxidative H_2O_2 and other radiolysis oxidants shifted OCP in a nobler direction.

<Figure 5>

3.4. Anodic polarization curves of zircaloy-2

3.4.1. Under irradiation condition

Measurement of anodic polarization curves was conducted using polished Zry-2 to investigate effect of radiated solution on pitting. **Figure 6** shows typical anodic polarization curves in ASW at room temperature at dose rates of 500 and 5000 Gy/h. As a reference, an anodic polarization curve for the no-radiation case was given. A breakdown of passivity, accompanied by a rapid increase in current density, was observed around 0.15 V. The difference in the pitting potentials with and without radiation was small: approximately 0.03 V. OCP at 500 Gy/h was slightly higher than for the no-radiation case, whereas OCP at 5000 Gy/h was remarkably higher. As seen in Figure 2, higher dose rates resulted in higher H_2O_2 production rates. After approximately 1 h of polarization measurements, 3 ppm and 1 ppm of H_2O_2 was generated at dose rates of 5000 Gy/h and 500 Gy/h, respectively. The effect of the presence of H_2O_2 would be demonstrated in changes in OCP.

3.4.2. Zircaloy-2 pre-irradiated in ASW

Measurement of anodic polarization curves was conducted using Zry-2 pre-irradiated in ASW at room temperature to investigate effect of surface film formed by irradiation on pitting. **Figure 7** shows typical anodic polarization curves of Zry-2 pre-irradiated at a dose rate of 5000 Gy/h for 50 and 100 h. As a reference, anodic polarization curves of Zry-2 pre-immersed in ASW for 0, 50, and 100 h at room temperature in the absence of radiation were also plotted. E_{pit} for pre-irradiated Zry-2 was higher than that for non-irradiated Zry-2. The current in the passive region (passive current density) for pre-irradiated Zry-2 was smaller than that for non-irradiated Zry-2. These results suggest that the oxide film became resistant to pitting corrosion during the gamma-ray irradiation.

<Figure 6>

<Figure 7>

3.5. Effect of chloride concentration on pitting potential

Figure 8 shows the relationship between chloride concentration and the pitting potential of Zry-2 obtained in diluted ASW at room temperature. Both the irradiated (dose rate of 500 and 5000 Gy/h) and non-irradiated cases were included. The measurements were carried out at least 5 times where the scattering of the data was taken into account, and the minimum value was plotted. The pitting potential increased with decreasing chloride concentrations in both the irradiated and non-irradiated cases. It is suggested that chloride is the main aggressive anion responsible for pitting corrosion of Zry-2, and pitting potential depends linearly on the logarithm of the chloride concentration.

<Figure 8>

3.6. Electrochemical impedance spectroscopy

Impedance data are plotted in the Nyquist and Bode plots for Zry-2 with different pre-irradiation time in ASW as shown in **Figure 9**. Before measurements were performed, Zry-2 specimens were irradiated in ASW at a dose rate of 5000 Gy/h for 0, 50, and 720 h. The impedance plots showed simple *R*-*C* behavior with a very high polarization resistance. Impedance data were analyzed and polarization resistance (R_p) and double layer capacitance (C_{dl}), and oxide film thickness (d) were calculated and tabulated in **Table 3**. The film thickness was calculated by Equation (3) [16];

$$d = \varepsilon \bullet \varepsilon_0 \bullet A / C_{dl} \quad (3)$$

where ε is the dielectric constant of the film which is taken as 22 assuming it as purely zirconium dioxide [17], ε_0 is the vacuum permittivity (8.85×10^{-14} F/cm), A is the effective surface area of

the sample and C_{dl} is the measured capacitance. The value of R_p was high with the order of MΩ•cm^2, and increased to some extent with pre-irradiation time. The high R_p indicates high corrosion resistance behavior of for Zry-2. The oxide film thickened by a long pre-irradiation time.

<Figure 9>

<Table 3>

3.7. XPS analysis of oxide film on zircaloy-2

XPS analysis of oxide films on Zry-2 was conducted to investigate the chemical state of elements and to compare the thickness of the oxide film. One sample was not immersed in ASW (blank sample), other samples were immersed in ASW at room temperature for 50, 100, and 720 h under irradiation at a dose rate of 5000 Gy/h.

Figure 10 shows the XPS spectra of Zr 3d and O 1s of Zry-2. The oxide films that formed on Zry-2 immersed in ASW were composed of zirconium oxides. As seen in Figure 10 (a), zirconium was combined with oxygen, giving peaks at 182.2 eV [18] and 184.5 eV [19] which are attributed to oxygen in ZrO_2. It was also found that the peak associated with metallic Zr (ca. 179 eV) diminished with increasing pre-irradiation time. Figure 10 (b) shows that oxygen was detected with oxidized states. The peak close to 530 eV was found to be composed of two peaks with the first peak (529.8 eV) corresponding to Zr-O oxygen (oxide oxygen) [20] and the second peak (531.7 eV) corresponding to oxygen in OH^- [19].

Figure 11 shows the composition profiles in the depth of Zry-2 immersed in ASW under irradiation at a dose rate of 5000 Gy/h. The sputtering rate was converted into depth using the results of SiO_2 sputtering. Film thickness was determined by the point which indicated the half oxygen content of the surface. **Table 4** summarizes the oxide film thickness obtained by the

above XPS analysis. The oxide film thickness was measured at 8.1 nm before immersion in ASW. Following immersion for 50, 100, and 720 h, the oxide film thickness was measured at 10.6, 11.6 and 13.4 nm in the case of irradiation. The thicknesses obtained by XPS and EIS analyses were different because the oxide film was assumed as purely zirconium dioxide in EIS analysis and surface roughness was omitted. However the oxide film formed on Zry-2 was thicker with irradiation time.

<Figure 10>

<Figure 11>

<Table 4>

3.8. H_2O_2 effect on oxide film formation and pit initiation

In this study, we focused on the radiolysis products generated in ASW. The main stable radiolysis product was H_2O_2. Oxide films formed on Zry-2 were found to be composed of zirconium oxide films as shown in Figure 11. It is considered that the oxide film was composed of two layers: at layer of oxide at the bulk material interface and a layer of hydroxide at the solution interface [21].

The interpretation for higher pitting potential could be that H_2O_2 thickens the oxide film on Zry-2. The corrosion resistance of Zry-2 results from its strong affinity for oxygen resulting in the spontaneous formation of a thin protective oxide film. Oxidation of Zry-2 continues to occur throughout the oxide film following anodic and cathodic reactions with a low oxidation current as shown in Figure 7. In order to simplify, Zry-2 is represented by the symbol Zr.

Cathodic sites reaction [13], [14]:

$$H_2O_2 + 2e^- \rightarrow 2OH^- \quad (4)$$

$$2H_2O + O_2 + 4e^- \rightarrow 4OH^- \quad (5)$$

Anodic site leading to oxide film thickening [22]:

$$Zr + 2H_2O \rightarrow ZrO_2 + 4H^+ + 4e^- \quad (6)$$

In the presence of gamma-rays, water (H_2O) decomposes to OH• radical and H• atom

by the following reaction:

$$H_2O \rightarrow 2OH\bullet + H\bullet \quad (7)$$

The OH• radical and H• atom can recombine to form H_2O_2, H_2, and water [23]:

$$OH\bullet + OH\bullet \rightarrow H_2O_2 \quad (8)$$

$$OH\bullet + H\bullet \rightarrow H_2O \quad (9)$$

$$H\bullet + H\bullet \rightarrow H_2 \quad (10)$$

Consumed H_2O_2 by cathodic reaction can immediately supply by water radiolysis. The oxide film can be form continuously.

Figure 6 shows that for a longer gamma-ray irradiation time the pitting potential shifts toward higher values and the passive current decreases accompanying H_2O_2 generation. H_2O_2, which is a highly oxidizing species, is capable of oxidizing the surface and limits pit initiation.

4. Conclusions

In order to evaluate the effects of radiolysis on pit initiation in zircaloy-2 in water containing sea salt, the pitting potentials of zircaloy-2 were measured using artificial seawater and a Co-60 gamma-ray source. The changes in composition of the water were analyzed. Furthermore, the oxide film formed on the zircaloy-2 surface was analyzed via electrochemical impedance spectroscopy and X-ray photoelectron spectroscopy. The following results were obtained:

(1) Under gamma-ray irradiation, hydrogen peroxide is the primary stable oxidizing radiolysis product in the water containing sea salt.

(2) The open circuit potential of zircaloy-2 under gamma-ray irradiation was nobler than in the case of non-irradiation because hydrogen peroxide could increase the oxidizing nature of the solution.

(3) Pitting potential decreased with increasing chloride concentration in both the presence and absence of gamma-ray irradiation. Chloride is the main aggressive anion responsible for pitting corrosion of Zry-2.

(4) Higher pitting corrosion potential was observed with longer irradiation time. The pitting potential was higher than open circuit potential.

(5) Under gamma-ray irradiation, the oxide film formed on the zircaloy-2 surface became thicker with irradiation time. The oxide film was resistant to pit initiation in the presence of chloride.

References

[1] http://www.meti.go.jp/earthquake/nuclear/pdf/120227_03aa.pdf, in Japanese, METI Measures and Requests in response to the Great East Japan Earthquake at home page of Ministry of Economy, Trade and Industry.

[2] http://www.tepco.co.jp/en/nu/fukushima-np/images/handouts_110825_02-e.pdf, handouts at press conference, Aug. 25, 2011, Tokyo Electronic Power Company.

[3] http://www.tepco.co.jp/en/nu/fukushima-np/images/handouts_121012_05-e.pdf, handouts at press conference, Oct. 12, 2012, Tokyo Electronic Power Company.

[4] Cox B. [Some thoughts on the mechanisms of in-reactor corrosion of zirconium alloys]. J. Nucl. Mater. 2005 Feb; 336: 331-368.

[5] Knittel DR, Maguire MA, Bronson A, Chen J. [The Effect of Surface Treatments and Electrochemical Methods on the Pitting Potentials of Zirconium in Chloride Solutions]. Corrosion. 1982 May; 38: 265-273.

[6] Palit GC, Gadiyar HS. [Pitting Corrosion of Zirconium in Chloride Solution]. Corrosion. 1987 Mar; 43: 140-148.

[7] Venkateswaran G. Pitting corrosion of zircaloy-2 in chloride media at 318 – 348K. Proc. 7th Int. Conf. Nucl. Eng.; 1999 Apr 19-23; Tokyo (Japan).

[8] Joseph JM, Choi BS, Yakabuskie P, Wren JC. [A combined experimental and model analysis on the effect of pH and O_2(aq) on γ-radiolytically produced H_2 and H_2O_2]. Radiat. Phys. and Chem. 2008 Sep; 77: 1009-1020.

[9] Kelm M, Bohnert E, A Kinetic Model for the Radiolysis of Chloride Brine, its Sensitivity against Model Parameters and a Comparison with Experiments. Karlsruhe (Germany): Forschungszentrum Karlsruhe in der Helmholtz-Gemeinschaft; 2004.

[10] Burns WG, Marsh WR, Walters WS. [The γ iraddation-enhansed corrosion of stainless and mild steels by water in the presence of air, argon and hydrogen]. Radiat. Phys. Chem. 1983 ; 21; 259-279.

[11] Motooka T, Sato T, Yamamoto M. [Effect of gamma-ray irradiation on the deoxygenation of salt-containing water using hydrazine]. J. Nucl. Sci and Tech. 2013; 50: 363-368.

[12] Sato N, Motooka T, Kato C, Yamamoto M. Corrosion phenomena in spent nuclear fuel storage pool containing salinity (1) determination of the corrosive environment by the water radiolysis calculation. Proc. 2012 Annual Meeting of AESJ: 2012 Mar. 27-29; Fukui (Japan). [CD ROM] [in Japanese]

[13] Pourbaix M. Atlas of Electrochemical Equilibria in Aqueous Solutions 2nd English Ed. Texas: NACE; 1974. p.112.

[14] Pourbaix M. Atlas of Electrochemical Equilibria in Aqueous Solutions 2nd English Ed. Texas: NACE; 1974. p.97.

[15] Kelm M, Bohnert E, [Radiation chemical effects in the near field of a final disposal site-I: radiolytic products formed in concentrated NaCl solutions]. Radio. Waste. Manag. Dispo 2000 Jan; 129: 119-122.

[16] Diggle JW. Downie TC. Goulding

CW. [The dissolution of porous oxide films on aluminium]. Electrochim. Acta. 1970 July; 15: 1079-1093.

[17] Bataillon C, Burunet S. [Electrochemical impedance spectroscopy on oxide films formed on zircaloy 4 in high temperature water]. Electrochim. Acta. 1994 Feb; 39: 455-465.

[18] Payen E, Gengembre L, Mauge F, Duchet JC, Lavalley JC. [Surface properties of zirconia catalyst carriers: interaction with oxomolybdates species]. Catalysis Today 1991 Nov; 10: 521-539.

[19] Majumdar D, Chatterjee D. [X-ray photoelectron spectroscopic studies on yttria, zirconia, and yttria-stabilized zirconia]. J. Appl. Phys. 1991 Jan; 70: 988-992.

[20] Barr TL. [An ESCA Study of Termination of the Passivation of Elemental Metals]. J. Phy. Chem. 1978; 82: 1801-1810.

[21] Meisterjahn P, Hoppe HW, Schultze JW. [Electrochemical and XPS measurements on thin

oxide films on zirconium]. J. Electroanal. Chem. Inter. Electrochem. 1987 Jan; 217: 159-185.

[22] Pourbaix M. Atlas of Electrochemical Equilibria in Aqueous Solutions 2nd English Ed. Texas: NACE; 1974. p.223.

[23] Le Caer S. [Water Radiolysis: Influence of Oxide Surfaces on H_2 Production under Ionizing Radiation]. Water. 2011; 3: 235-253.

Figure captions

Figure 1. Schematic illustration of a zircaloy-2 specimen for electrochemical measurements. Zry-2: zircaloy-2, Zr: zirconium.

Figure 2. Changes in H_2O_2 concentrations in artificial seawater at room temperature under gamma-ray irradiation for 100 h at a dose rate of 500 and 5000 Gy/h. ASW: artificial seawater, RT: room temperature.

Figure 3. Chromatogram of artificial seawater after 100 h of gamma-ray irradiation at a dose rate of 5000 Gy/h at room temperature.

Figure 4. Cathodic polarization curves of platinum in artificial seawater, with and without 30 ppm of H_2O_2. Test solutions contain 6.5 ppm of DO. SSE: saturated KCl Ag/AgCl electrode, OCP: open circuit potential, DO: dissolved oxygen.

Figure 5. Changes in open circuit potentials of zircaloy-2 in artificial seawater under gamma-ray irradiation at dose rates of 500 and 5000 Gy/h, and in the absence of radiation in ASW with and without 30 ppm of H_2O_2 at room temperature. Dotted lines indicate the case of non-irradiation and solid lines indicate the presence of radiation.

Figure 6. Typical anodic polarization curves of zircaloy-2 obtained in artificial seawater at room temperature in the presence of radiation at dose rates of 500 and 5000 Gy/h and in the absence of radiation.

Figure 7. Typical anodic polarization curves of zircaloy-2 pre-irradiated in artificial seawater at a dose rate of 5000 Gy/h for 50 and 100 h at room temperature and immersed in artificial seawater for 0, 50, and 100 h. Solid lines indicate data for pre-irradiated specimens. Dotted lines indicate data for specimens that had not been irradiated.

Figure 8. Pitting potential of zircaloy-2 in diluted artificial seawater at room temperature under gamma-ray irradiation at dose rates of 500 and 5000 Gy/h as well as in the absence of radiation. Open marks indicate data in which radiation was present and closed marks indicate data taken in the absence of radiation.

Figure 9. (a) Nyquist plots of zircaloy-2 in ASW at OCP. (b) Bode plots of zircaloy-2 in ASW at OCP. Zircaloy-2 was irradiated for 0, 50, and 720 h prior to EIS measurements.

Figure 10. (a) Zr 3d spectra and (b) O 1s spectra for zircaloy-2 immersed in artificial seawater at room temperature in both the presence and absence of radiation. (1) No irradiation, (2) Irradiation at 5000 Gy/h for 50 h, (3) Irradiation at 5000 Gy/h for 100 h, (4) Irradiation at 5000 Gy/h for 720 h.

Figure 11. Composition profiles in the depth of zircaloy-2, (a) before immersion, (b) immersed for 50 h, (c) immersed for 100 h, and (d) immersed for 720 h in the presence of radiation at a dose rate of 5000 Gy/h in artificial seawater at room temperature.

Table captions

Table 1. Chemical composition of artificial seawater (ppm).

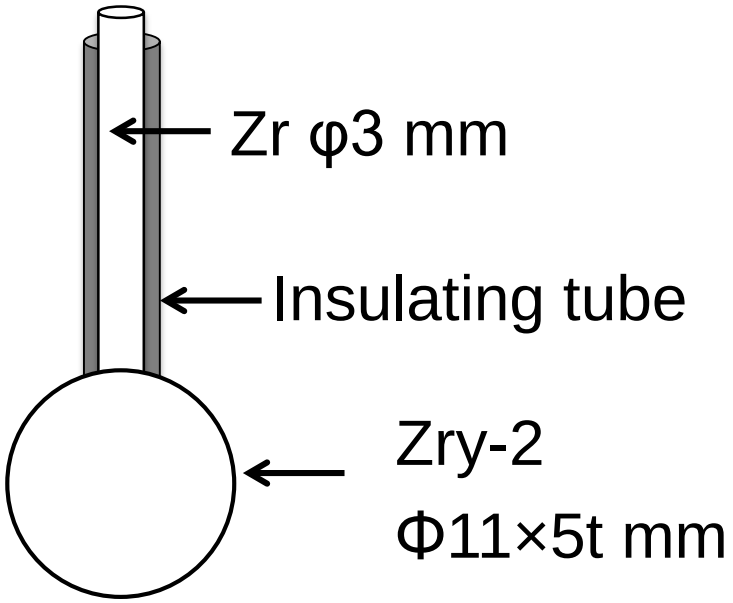

Figure 1. Schematic illustration of a zircaloy-2 specimen for electrochemical measurements. Zry-2: zircaloy-2, Zr: zirconium.

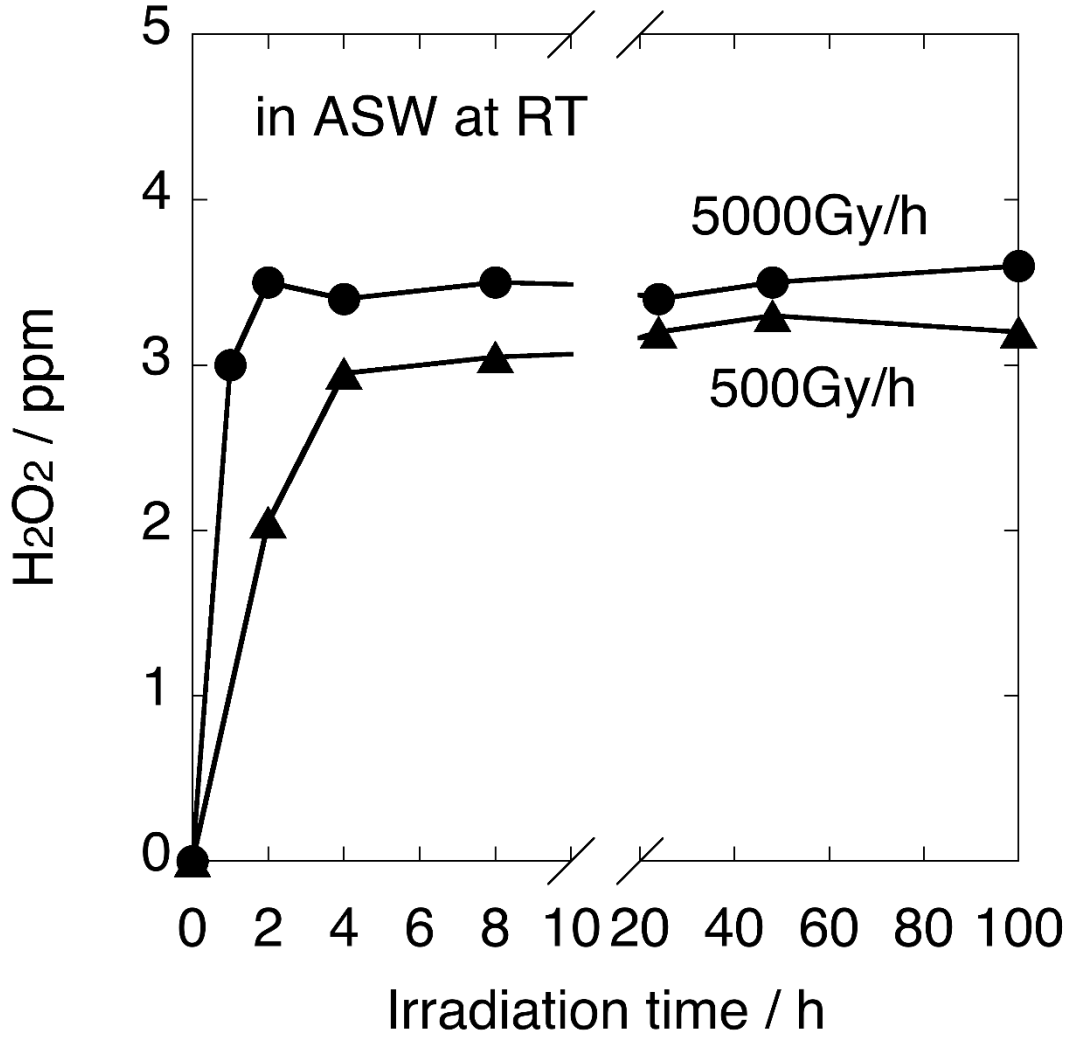

Figure 2. Changes in H_2O_2 concentrations in artificial seawater at room temperature under gamma-ray irradiation for 100 h at a dose rate of 500 and 5000 Gy/h. ASW: artificial seawater, RT: room temperature.

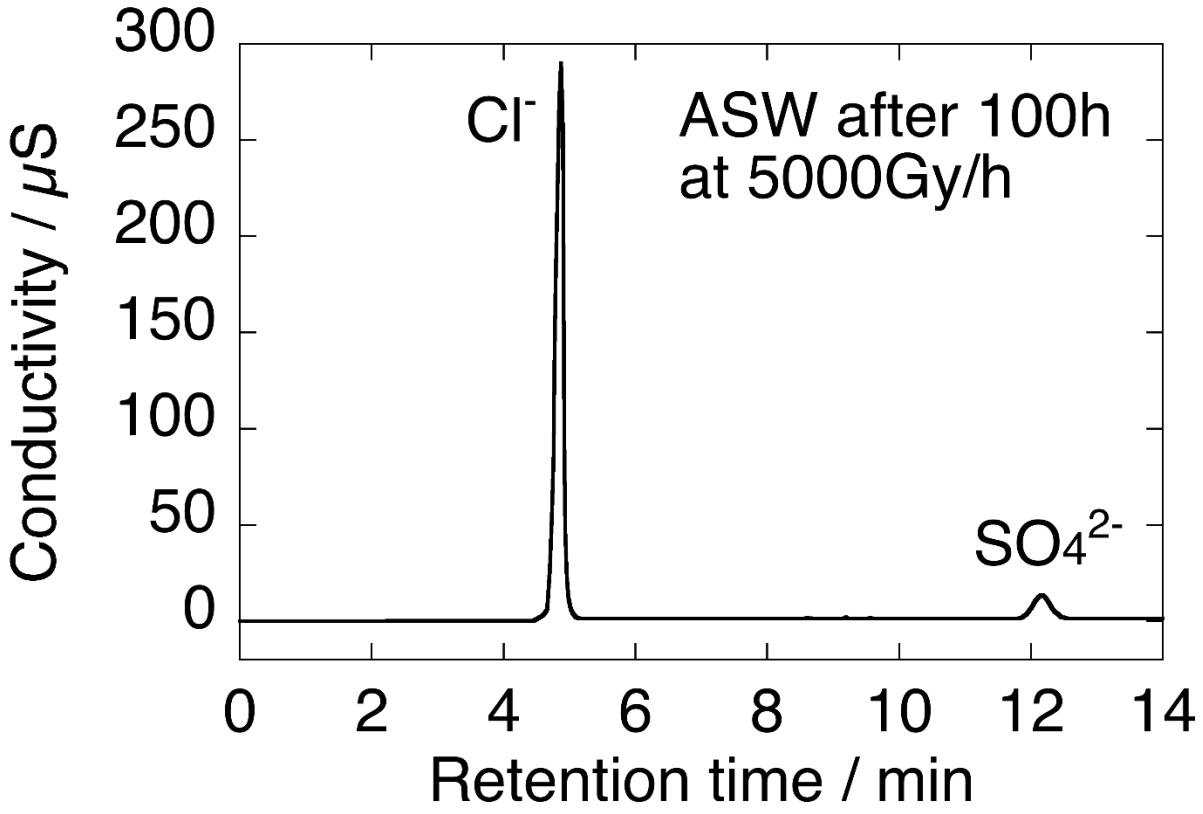

Figure 3. Chromatogram of artificial seawater after 100 h of gamma-ray irradiation at a dose rate of 5000 Gy/h at room temperature.

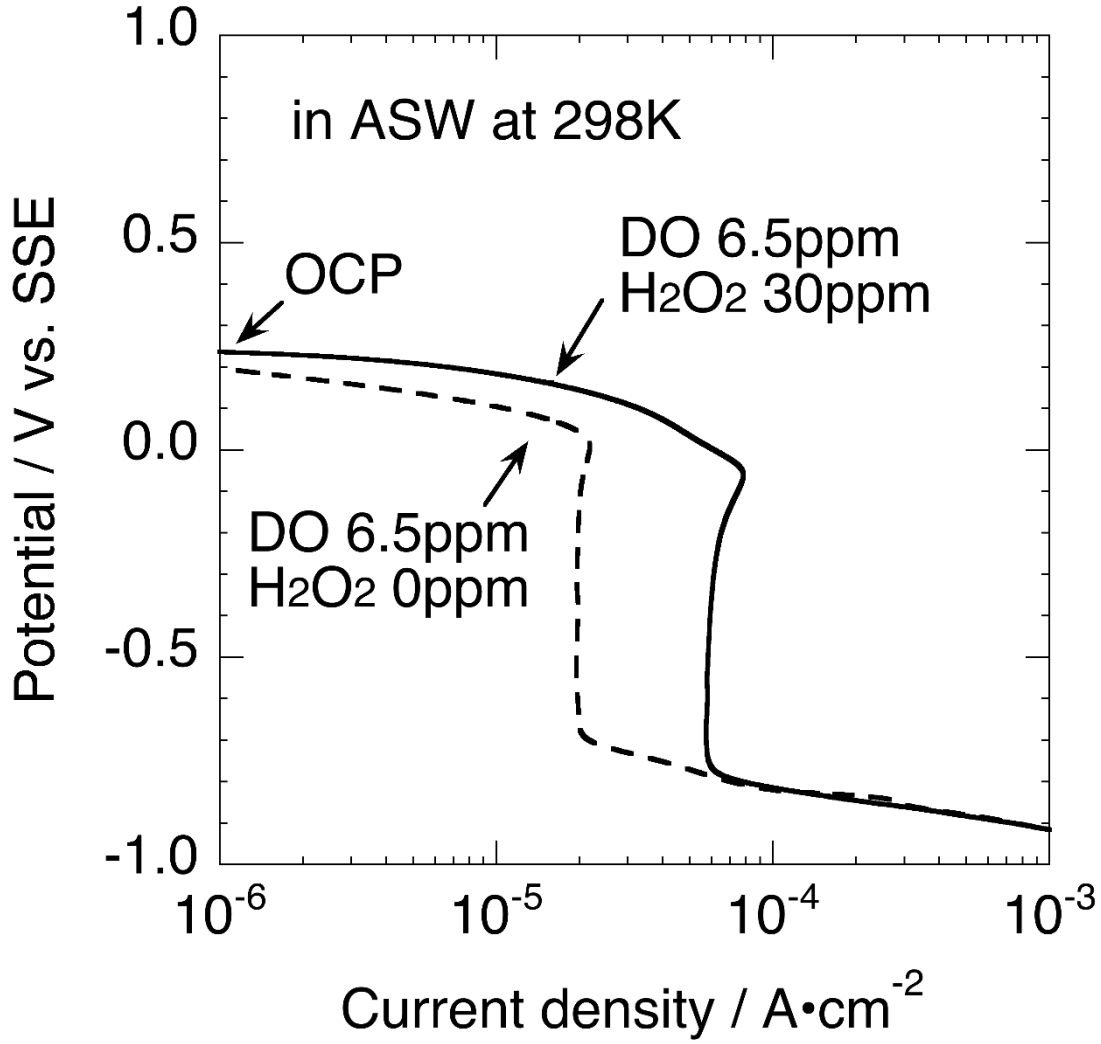

Figure 4. Cathodic polarization curves of platinum in artificial seawater, with and without 30 ppm of H_2O_2. Test solutions contain 6.5 ppm of DO. SSE: saturated KCl Ag/AgCl electrode, OCP: open circuit potential, DO: dissolved oxygen.

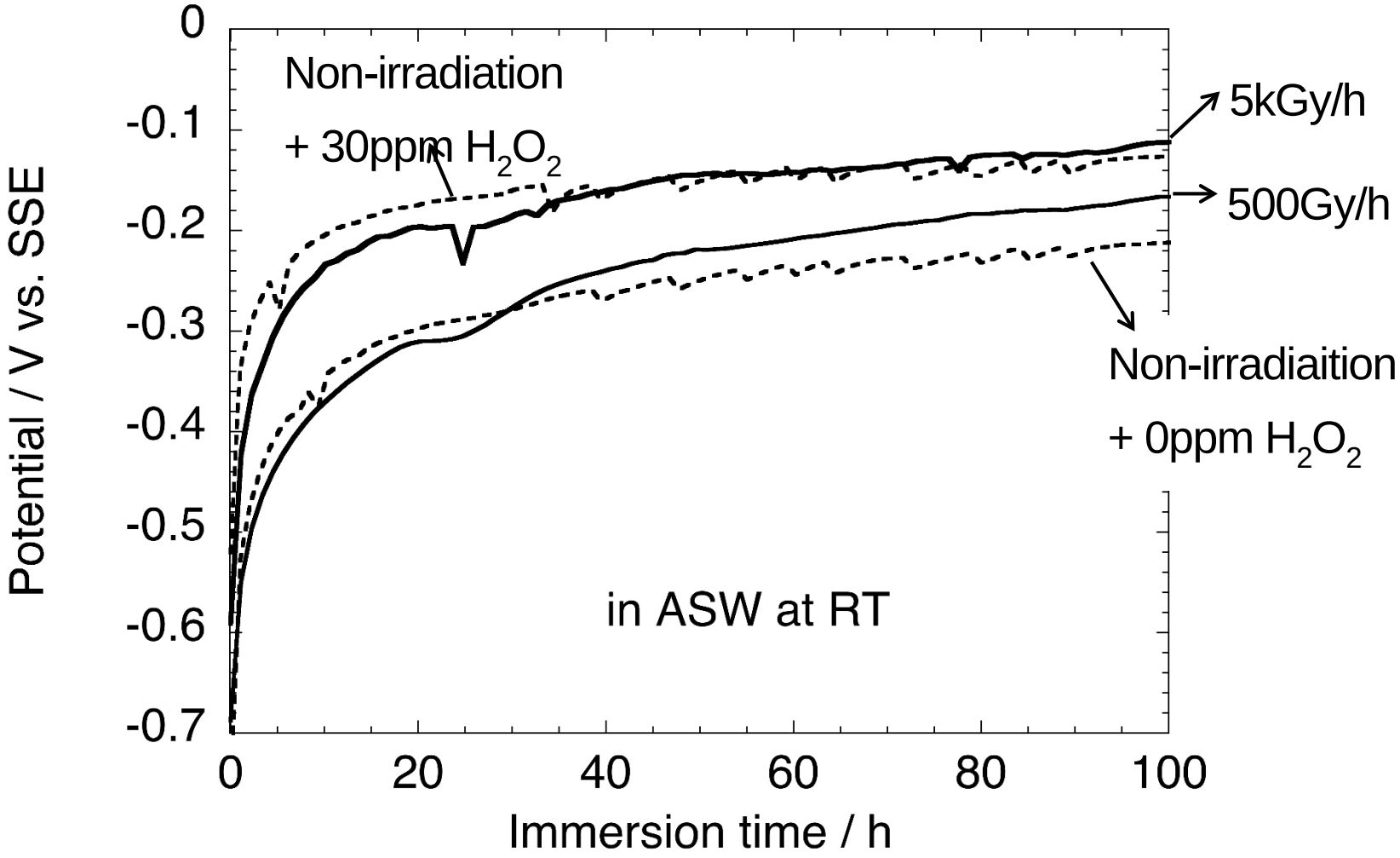

Figure 5. Changes in open circuit potentials of zircaloy-2 in artificial seawater under gamma-ray irradiation at dose rates of 500 and 5000 Gy/h, and in the absence of radiation in ASW with and without 30 ppm of H_2O_2 at room temperature. Dotted lines indicate the case of non-irradiation and solid lines indicate the presence of radiation.

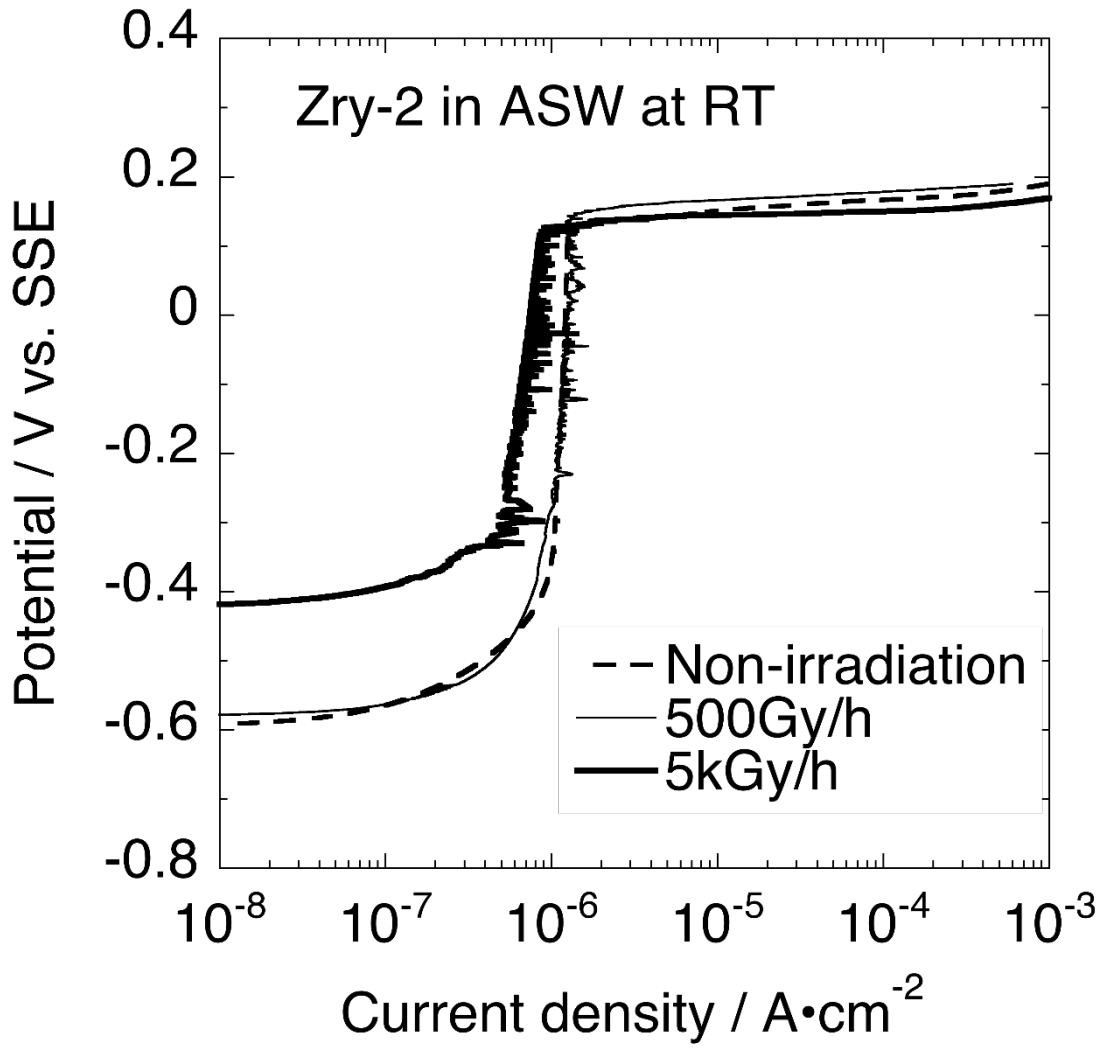

Figure 6. Typical anodic polarization curves of zircaloy-2 obtained in artificial seawater at room temperature in the presence of radiation at dose rates of 500 and 5000 Gy/h and in the absence of radiation.

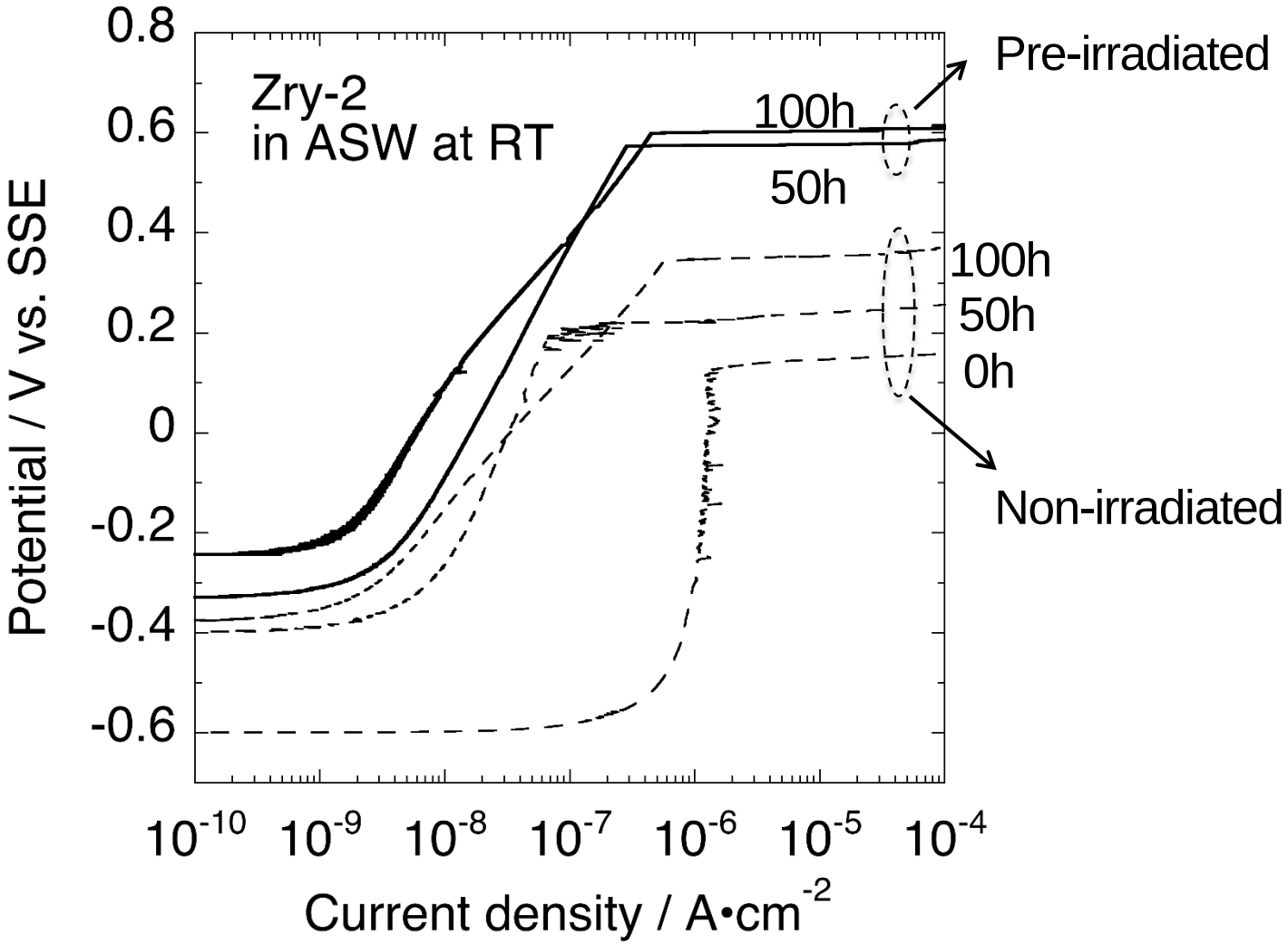

Figure 7. Typical anodic polarization curves of zircaloy-2 pre-irradiated in artificial seawater at a dose rate of 5000 Gy/h for 50 and 100 h at room temperature and immersed in artificial seawater for 0, 50, and 100 h. Solid lines indicate data for pre-irradiated specimens. Dotted lines indicate data for specimens that had not been irradiated.

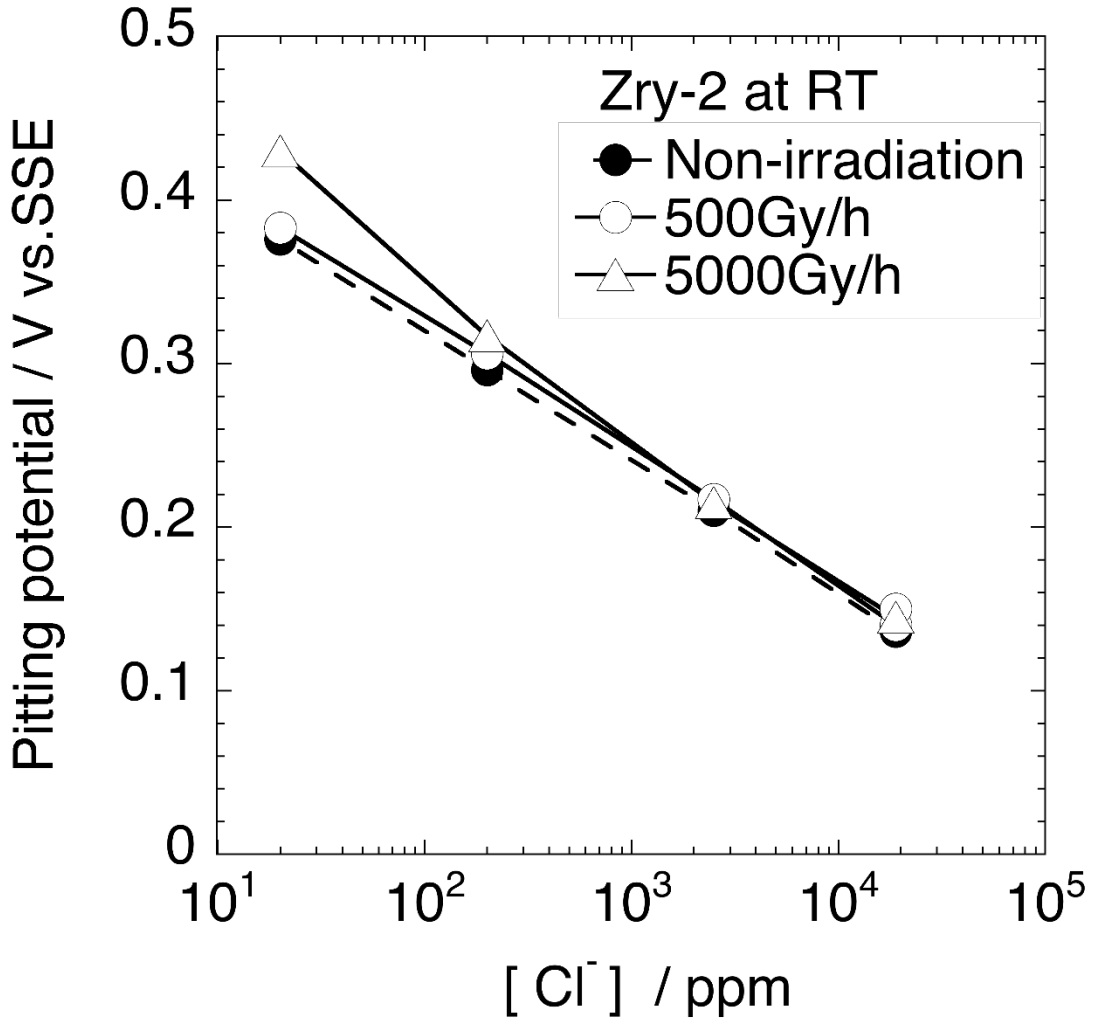

Figure 8. Pitting potential of zircaloy-2 in diluted artificial seawater at room temperature under gamma-ray irradiation at dose rates of 500 and 5000 Gy/h as well as in the absence of radiation. Open marks indicate data in which radiation was present and closed marks indicate data taken in the absence of radiation.

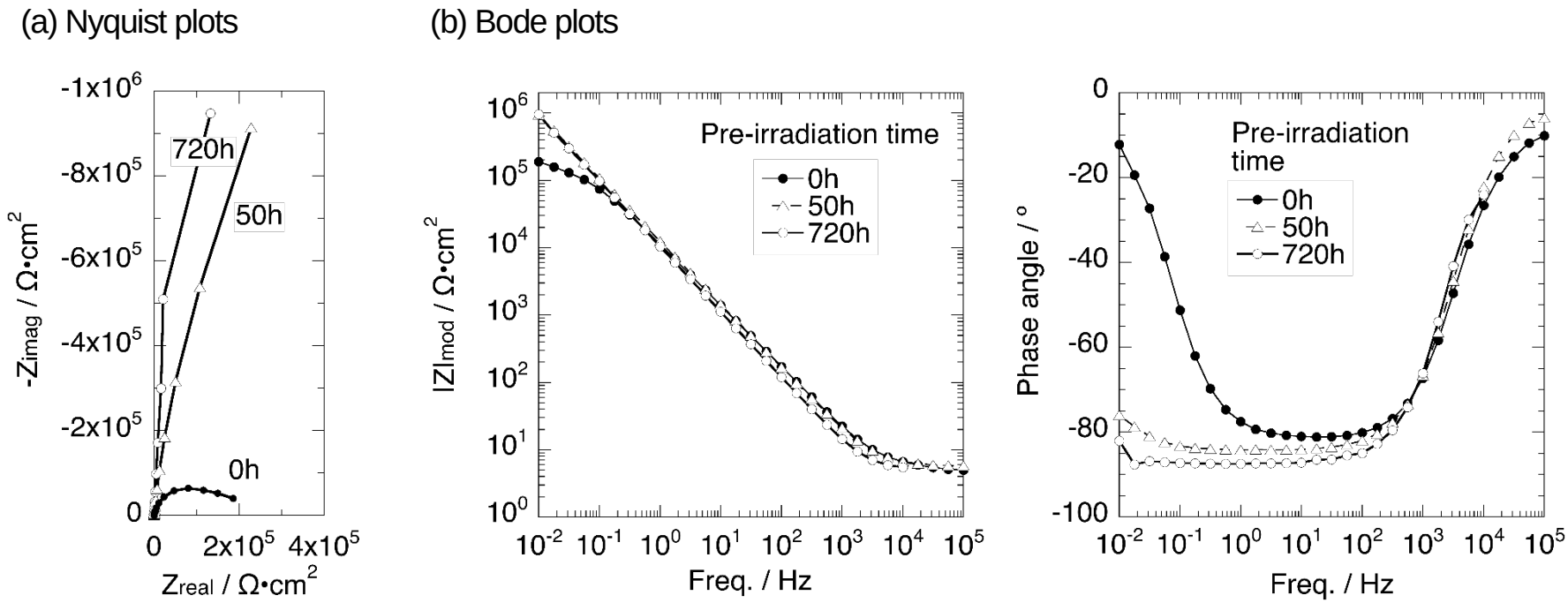

Figure 9. (a) Nyquist plots of zircaloy-2 in ASW at OCP. (b) Bode plots of zircaloy-2 in ASW at OCP. Zircaloy-2 was irradiated for 0, 50, and 720 h prior to EIS measurements.

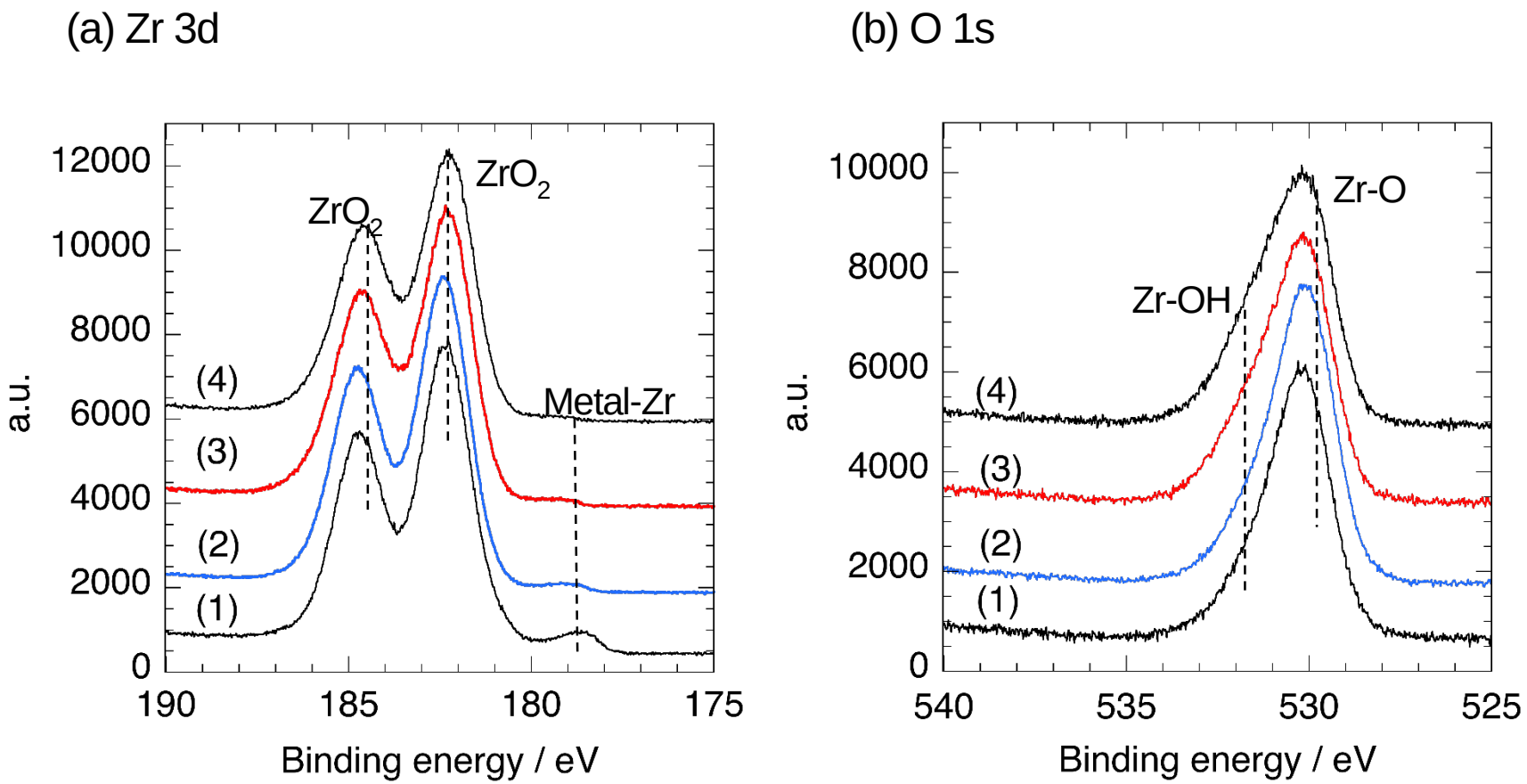

Figure 10. (a) Zr 3d spectra and (b) O 1s spectra for zircaloy-2 immersed in artificial seawater at room temperature in both the presence and absence of radiation. (1) No irradiation, (2) Irradiation at 5000 Gy/h for 50 h, (3) Irradiation at 5000 Gy/h for 100 h, (4) Irradiation at 5000 Gy/h for 720 h.

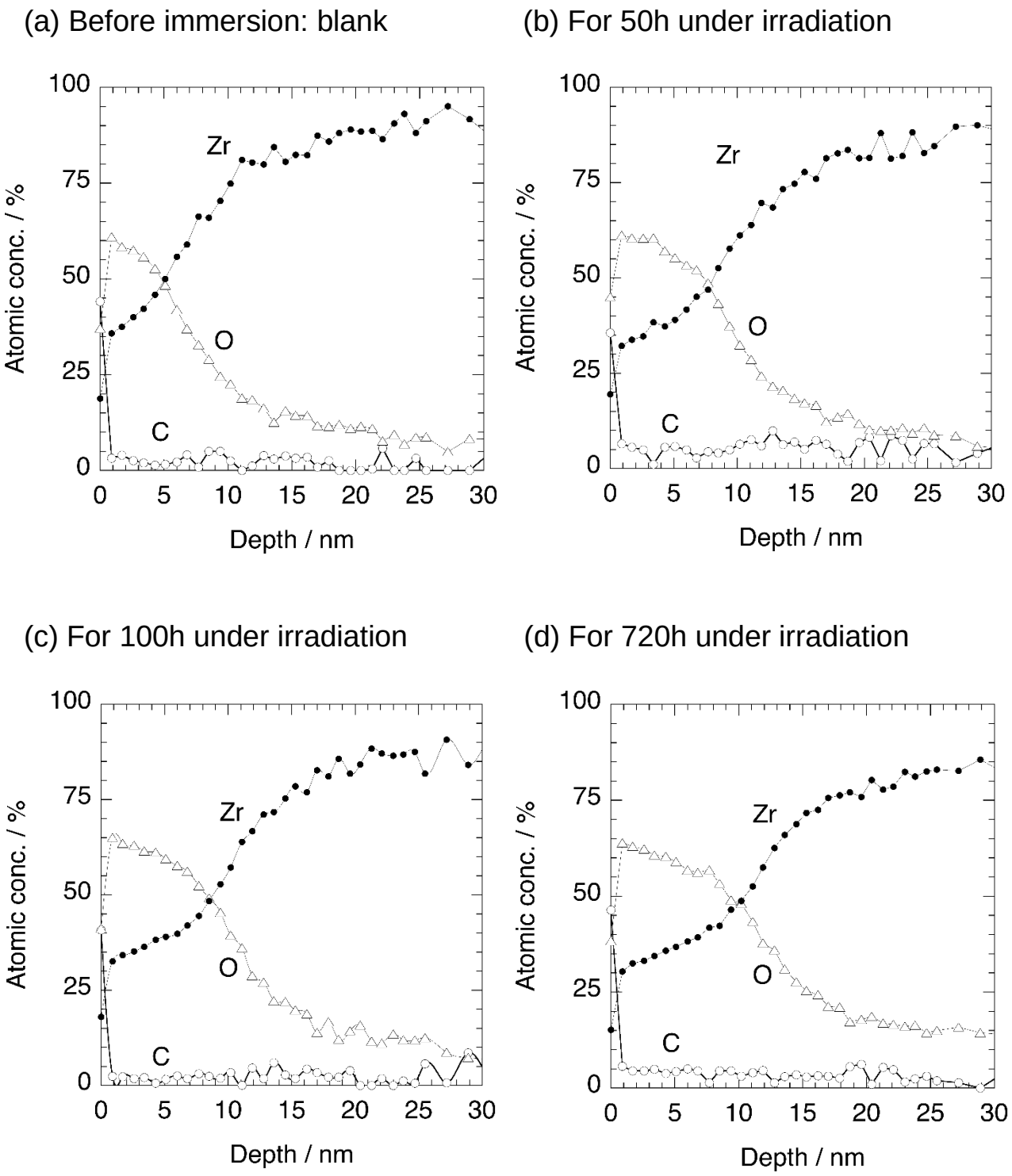

Figure 11. Composition profiles in the depth of zircaloy-2, (a) before immersion, (b) immersed for 50 h, (c) immersed for 100 h, and (d) immersed for 720 h in the presence of radiation at a dose rate of 5000 Gy/h in artificial seawater at room temperature.

Table 1. Chemical composition of artificial seawater (ppm).

Cl^-	SO_4^{2-}	HCO_3^-	Br^-	Na^+	Mg^{2+}	Ca^{2+}
19000	2650	140	64	10600	1300	400

Table 2. Chemical composition of zircaloy-2 rod (mass%).

Sn	Fe	Cr	Ni	O	H	Zr
1.43	0.12	0.11	0.053	0.12	0.0008	Bal.

Table 3. Polarization resistance (R_p), double layer capacitance (C_{dl}) and film thickness (d) computed from EIS data on zircaloy-2 in ASW with different periods of time at a dose rate of 5000 Gy/h.

Pre-irradiated time (hour)	*Rp* ($M\Omega \cdot cm^2$)	*Cdl* ($\mu F/cm^2$)	Thickness (nm)
0	0.34	15.4	4.6
50	3.6	13.6	5.2
720	6.8	11.5	6.1

Table 4. Oxide film thickness obtained by XPS analysis (nm).

Immersion condition	Immersion time / h			
	0	50	100	720
Irradiation at 5kGy/h	8.1	10.6	11.6	13.4